

AN IMPRINT OF SUPER-STRUCTURES ON THE MICROWAVE BACKGROUND DUE TO THE INTEGRATED SACHS-WOLFE EFFECT

BENJAMIN R. GRANETT, MARK C. NEYRINCK AND ISTVÁN SZAPUDI
Institute for Astronomy, University of Hawaii, 2680 Woodlawn Drive, Honolulu HI 96822
Draft version October 23, 2018

ABSTRACT

We measure hot and cold spots on the microwave background associated with supercluster and supervoid structures identified in the Sloan Digital Sky Survey Luminous Red Galaxy catalog. The structures give a compelling visual imprint, with a mean temperature deviation of $9.6 \pm 2.2 \mu\text{K}$, i.e. above 4σ . We interpret this as a detection of the late-time Integrated Sachs-Wolfe (ISW) effect, in which cosmic acceleration from dark energy causes gravitational potentials to decay, heating or cooling photons passing through density crests or troughs. In a flat universe, the linear ISW effect is a direct signal of dark energy.

Subject headings: cosmic microwave background — cosmology: observations — large-scale structure of universe — methods: statistical

1. INTRODUCTION

The cosmic microwave background (CMB) is a snapshot of the early universe; however, the light we observe has been processed by large-scale structure at low redshift, in part through the late-time integrated Sachs-Wolfe (ISW) effect (Sachs & Wolfe 1967). As photons travel through time-varying gravitational potentials, they are slightly heated or cooled. In a universe dominated by dark energy, the gravitational potential decays with time even in linear theory, heating photons traveling through crests and cooling photons in troughs of large-scale matter density fluctuations. Hereafter, ‘ISW’ refers to the full nonlinear late-time ISW effect, also known as the Rees-Sciama effect (Rees & Sciama 1968).

The ISW effect from dark energy can be detected with the cross-correlation function between the projected galaxy density and microwave background temperature over the sky (Crittenden & Turok 1996). Measurements from individual galaxy surveys detect the effect with signal-to-noise no higher than 3 (Scranton et al. 2003; Boughn & Crittenden 2004; Afshordi et al. 2004; Padmanabhan et al. 2005; Raccanelli et al. 2008). Recently, various groups have combined multiple datasets to arrive at a detection as high as 4.5σ , though error estimation with correlated galaxy datasets complicates the physical interpretation (Ho et al. 2008; Giannantonio et al. 2008). Additionally, studies using wavelet analyses have suggested that the signal can be localized to particular regions on the sky that depend on both the CMB and the galaxy density (McEwen et al. 2008).

The ISW signal peaks at spherical multipole $\ell \sim 20$ at $z = 0.5$ in the galaxy-CMB cross-power spectrum $\ell(\ell+1)C_\ell$ (e.g. Padmanabhan et al. 2005). This corresponds to structures with angular radius $\sim 4^\circ$, or $\sim 100 h^{-1}\text{Mpc}$. We call these large structures ‘supervoids’ and ‘superclusters,’ but they may be thought of as gentle hills and valleys in the linear density field. In a ΛCDM universe, the ISW signal from these broad, linear over- or under-dense structures is expected to dominate over smaller-scale fluctuations in the density.

In this study, we identified a sample of supervoids and superclusters in a galaxy survey that could potentially produce measurable ISW signals. We analyze these structures by stacking cutouts of the CMB centered on their projected locations. Atrio-Barandela et al. (2008) recently used a sim-

ilar method on much smaller spatial scales, stacking WMAP data behind clusters to detect the frequency-dependent thermal Sunyaev-Zeldovich (Sunyaev & Zeldovich 1972) effect. We show that our structures are, on average, associated with a significant temperature imprint on the CMB. This is arguably the first visually compelling detection of the ISW effect. In our conclusions, we discuss the application of this work to dark energy and analysis of secondary CMB anisotropies.

2. DATA AND METHODOLOGY

We used a sample of 1.1 million Luminous Red Galaxies (LRGs) from the Sloan Digital Sky Survey (SDSS) (Adelman-McCarthy et al. 2008) covering 7500 square degrees about the North Galactic pole. They span a redshift range of $0.4 < z < 0.75$, with a median of ~ 0.5 , and inhabit a volume of about $5 h^{-3}\text{Gpc}^3$. LRGs are elliptical galaxies in massive galaxy clusters representing large dark-matter halos (Blake et al. 2008), and are thought to be physically similar objects across their redshift range (Eisenstein et al. 2001; Wake et al. 2008). This makes them excellent, albeit sparse, tracers of the cosmic matter distribution on scales $\gtrsim 10\text{Mpc}$. Our sample was selected from photometric data based on the criteria used in the Mega-Z LRG catalog over the SDSS Data Release 4 footprint (Collister et al. 2007). We remove sources classified as stars in the SDSS catalog, but do not use the star/galaxy classifier in the MegaZ catalog. Contamination by stars is estimated by Collister et al. (2007) to be 5%. We extended the catalog with the additional area from Data Release 6. Redshifts for the new area were estimated by a nearest neighbor match with the *ugriz* photometry. We estimate that this procedure smooths the redshift distribution by $\sigma_z = .003$ and has little effect on the overall redshift uncertainty, which is at the $\sigma_z = .05$ level.

The CMB temperature map we used is an inverse-variance weighted combination of the *Wilkinson Microwave Anisotropy Probe* (WMAP) 5-year Q, V and W frequency maps (Hinshaw et al. 2008), with the foreground galactic-emission maps subtracted from each. Regions within the extended temperature analysis mask (KQ75), which is a conservative Galactic and point source mask, are left out of the analysis. The maps are pixelized in Healpix format (Górski et al. 2005) at 7 arcminute resolution, which oversamples the 30-arcminute full-width, half-max beam. In excellent agreement

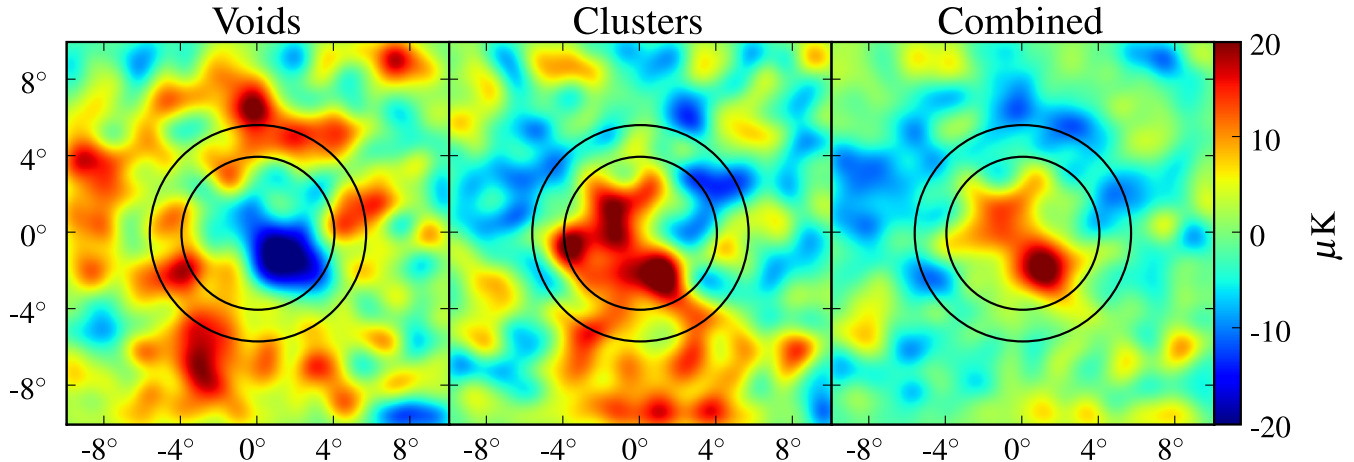


FIG. 1.— Stacked regions on the CMB corresponding to supervoid and supercluster structures identified in the SDSS LRG catalog. We averaged CMB cut-outs around 50 supervoids (left) and 50 superclusters (center), and the combined sample (right). The cut-outs are rotated, to align each structure’s major axis with the vertical direction. Our statistical analysis uses the raw images, but for this figure we smooth them with a Gaussian kernel with FWHM 1.4° . Hot and cold spots appear in the cluster and void stacks, respectively, with a characteristic radius of 4° , corresponding to spatial scales of $100 h^{-1}\text{Mpc}$. The inner circle (4° radius) and equal-area outer ring mark the extent of the compensated filter used in our analysis. Given the uncertainty in void and cluster orientations, small-scale features should be interpreted cautiously.

with previous results (Giannantonio et al. 2008), we measured a cross-correlation amplitude between our two data sets on 1° scales of $0.7\mu\text{K}$.

To find supervoids in the galaxy sample, we used the parameter-free, publicly available ZOBOV (ZOnes Bordering On Voidness; Neyrinck 2008) algorithm. For each galaxy, ZOBOV estimates the density and set of neighbors using the parameter-free Voronoi tessellation (Okabe et al. 2000; van de Weygaert & Schaap 2007). Then, around each density minimum, ZOBOV finds density depressions, i.e. voids. We used VOBOZ (Neyrinck, Gnedin & Hamilton 2005) to detect clusters, the same algorithm applied to the inverse of the density.

In 2D, if density were represented as height, the density depressions ZOBOV finds would correspond to catchment basins (e.g. Platen, van de Weygaert & Jones 2007). Large voids can include multiple depressions, joined together to form a most-probable extent. This requires judging the significance of a depression; for this, we use its density contrast, comparing against density contrasts of voids from a uniform Poisson point sample. Most of the voids and clusters in our catalog consist of single depressions.

We estimated the density of the galaxy sample in 3D, converting redshift to distance according to WMAP5 (Komatsu et al. 2008) cosmological parameters. To correct for the variable selection function, we normalized the galaxy densities to have the same mean in 100 equally spaced distance bins. This also removes almost all dependence on the redshift-distance mapping that the galaxy densities might have. We took many steps to ensure that survey boundaries and holes did not affect the structures we detected. We put a 1° buffer of galaxies (sampled at thrice the mean density) around the survey footprint, and put buffer galaxies with maximum separation 1° from each other in front of and behind the dataset. Any real galaxies with Voronoi neighbors within a buffer were not used to find structures. We handled survey holes (caused by bright stars, etc.) by filling them with random fake galaxies at the mean density. The hole galaxies comprise about 1/300 of the galaxies used to find voids and clusters. From the final

cluster and void lists, we discarded any structures that overlapped LRG survey holes by $\geq 10\%$, that were $\leq 2.5^\circ$ (the stripe width) from the footprint boundary, that were centered on a WMAP point source, or that otherwise fell outside the boundaries of the WMAP mask.

We found 631 voids and 2836 clusters above a 2σ significance level, evaluated by comparing their density contrasts to those of voids and clusters in a uniform Poisson point sample. There are so many structures because of the high sensitivity of the Voronoi tessellation. Most of them are spurious, arising from discreteness noise. We used only the highest-density-contrast structures in our analysis; we discuss the size of our sample below.

We defined the centers of structures by averaging the positions of member galaxies, weighting by the Voronoi volume in the case of voids. The mean radius of voids, defined as the average distance of member galaxies from the center, was 2.0° ; for clusters, the mean radius was 0.5° . The average maximum distance between void galaxies and centers was 4.0° ; for clusters, it was 1.1° . For each structure, an orientation and ellipticity is measured using the moments of the member galaxies, though it is not expected that this morphological information is significant, given the galaxy sparseness.

3. IMPRINTS ON THE CMB

Figure 1 shows a stack image built by averaging the regions on the CMB surrounding each object. The CMB stack corresponding to supervoids shows a cold spot of $-11.3\mu\text{K}$ with 3.7σ significance, while that corresponding to superclusters shows a hot spot of $7.9\mu\text{K}$ with 2.6σ significance, assessed in the same way as for the combined signal, described below. Figure 2 shows a histogram of the signals from each void and cluster.

To assess the significance of our detection, we averaged the negative of the supervoid image with the supercluster image, expecting that the voids would produce an opposite signal from the clusters. We used a top-hat compensated filter to measure the fluctuations, averaging the mean temperature

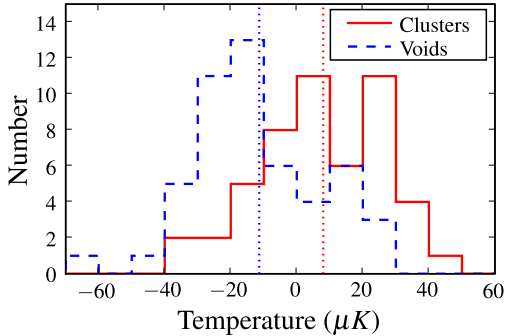


FIG. 2.— Histograms of the signals of the 50 highest-significance supervoids and superclusters used for our detection, measured in our compensated filter. The vertical dotted lines are the means of each distribution, at $-11.3 \pm 3.1 \mu\text{K}$ (voids) and $7.9 \pm 3.1 \mu\text{K}$ (clusters).

within 4° of the center, and then subtracting the mean temperature in a ring of the same area around it. This filter is insensitive to CMB fluctuations on scales larger than the object detected; for an uncompensated filter, these fluctuations would constitute a significant source of noise.

What is the likelihood that our results are due to random fluctuations? To estimate that, we performed two sets of 1000 Monte Carlo simulations. First, we generated random positions of voids and clusters within the survey and stacked the corresponding areas of the actual CMB map. This models the errors given the observed CMB sky and foreground subtraction, but might not properly account for any covariance due to the actual configuration of voids and clusters. Second, we generated model CMB skies smoothed to WMAP resolution and repeated our analysis on these with the actual void and cluster configurations observed in the catalogs. We find that these two approaches produce identical distributions consistent with Gaussians, and with standard deviations within 2% of each other. The hypothesis that the signal arose from random fluctuations is excluded at the 4.4σ level, a 1:200,000 chance. Our final mean signal with errors is $9.6 \pm 2.2 \mu\text{K}$.

We note that the radii of the structures found by ZOBOV/VOBOZ are typically less than 4° . One possible reason is that the algorithm could be conservative in defining edges in the face of significant discreteness noise. The detected structures could just be the tips of larger hills and valleys in the potential. The stacked signal is also likely smeared somewhat from noise in determining the structures' centers.

Our procedure does have two parameters: the number of objects used to generate the stacked image, and the filter size used to assess the hot and cold spots' significance. We used the same number of voids and clusters for simplicity. Density-contrast thresholds of 4, 3 and 2σ give 7, 51, and 631 voids, respectively. With too few structures, the measurement would be swamped by CMB fluctuations (with a standard deviation of $22 \mu\text{K}$ in our filter). With too many, structures would be introduced that have dubious physicality. We used the 50 objects with the highest density contrast (a cut at $\sim 3\sigma$ for voids, and $\sim 3.3\sigma$ for clusters) to roughly balance these effects. Stacking 70 voids and clusters gives a signal of 2.8σ ; with 30, the signal remains above 4σ . These results appear in Table 1. It is almost certain that some number of objects would give a higher significance than 50 gives, but we did not search this parameter space, to simplify the interpretation.

As mentioned earlier, the ISW signal is expected to peak at a radius of $\sim 4^\circ$ according to theory; this is also confirmed

TABLE 1
DEPENDENCE ON NUMBER AND RADIUS.

N	Radius	$\Delta T \mu\text{K}$	$\Delta T/\sigma$
30	4.0°	11.1	4.0
50	4.0°	9.6	4.4
70	4.0°	5.4	2.8
50	3.0°	8.4	3.4
50	3.5°	9.3	4.0
50	4.0°	9.6	4.4
50	4.5°	9.2	4.4
50	5.0°	7.8	3.8

by the visual appearance of the images. Changing the filter radius between $3-5^\circ$ results in various detection significances of approximately 4σ ; these results are listed in Table 1. In a strict Bayesian sense, even inspecting the image by eye prior to statistical analysis complicates the interpretation due to *a posteriori* bias issues. This would be difficult to quantify, but its effect should be small because the signal was robust in the few cases we checked.

There are systematic effects from foreground contamination that, in principle, can mimic the ISW signal. Dust emission from the Milky Way is bright at microwave frequencies and is correlated with the dust extinction correction used in the galaxy catalog. Extragalactic radio sources correlated with luminous red galaxies could also potentially contribute to a false signal at microwave frequencies. To check that we are not significantly contaminated by microwave sources, we repeated our analysis on the individual frequency maps using the KQ75 mask as in our combined analysis, but without subtracting the foreground template maps. The mean amplitudes of the void signal in the Q, V and W bands were -10.6 , -11.1 and $-11.1 \mu\text{K}$; the mean amplitudes of the cluster signal were 7.8 , 7.9 and $7.7 \mu\text{K}$; the error on each of these means is $3.1 \mu\text{K}$. These results agree with our measurement made on the combined map, and demonstrate that there is no significant frequency dependence of the signal. Moreover, the void signal is expected to be less sensitive to foreground contamination.

4. DISCUSSION

We have measured a 4σ temperature deviation on the CMB due to supervoids and superclusters at $z \sim 0.5$. The most likely explanation for this is that we detect the ISW effect. The linear ISW effect vanishes in a flat universe without dark energy, and the higher-order ISW contribution is expected to be significantly lower than the ISW in ΛCDM (Seljak 1996; Tuluie et al. 1996; Crittenden & Turok 1996). The consensus in the literature is that detecting the ISW effect signals the presence of dark energy in a flat Universe.

To estimate the expected effect from ISW in a ΛCDM universe, we measured the signal that the Millennium cosmological N -body simulation (Springel et al. 2005) produces. We ray-traced through the simulation, summing up the change in potential that a photon would experience passing through the $500 h^{-1}\text{Mpc}$ box in each Cartesian direction. In this volume, which is large enough for 1 or 2 supervoids and superclusters, we checked that the linear part of the ISW signal through the box dominates over higher-order effects. Centering a $100 h^{-1}\text{Mpc}$ aperture around the maximum ISW signal in the Millennium volume gives $4.2 \mu\text{K}$, $\sim 2\sigma$ lower than what we observed in our CMB stack. Though we only expect these numbers to agree to within an order of magnitude, we note that most previous ISW measurements are also some-

what higher than the predicted signal in a Λ CDM cosmology (Ho et al. 2008). While more theoretical studies are needed to turn our detection into precision constraints on cosmological parameters, we interpret our image as the ISW effect on the CMB caused by the decaying of potentials in an accelerating universe with dark energy.

Previous works used the two-point cross-correlation function of 2D projected galaxy density maps with the CMB to detect the ISW effect, reaching a significance of 2 to 2.5σ for the galaxy sample we analyzed (Ho et al. 2008; Giannantonio et al. 2008). Several factors likely contribute to the higher significance of our measurement. First, we analyze only superstructures that should be strong ISW sources. Second, we use 3D information to identify them. The 2D projected galaxy density is typically not extremal at the superstructures' locations; thus, the cross-correlation function is not especially sensitive to their contributions. Third, galaxy autocorrelations directly contribute to the noise for the cross-correlation function, but not for our method.

Our detection makes it more plausible that low-redshift supervoids and superclusters explain anomalies observed on the CMB (Rakić et al. 2006; Rudnick et al. 2007; Inoue & Silk 2007; Maturi et al. 2007). At low to moderate significance, these features include a 5° $70\mu\text{K}$ cold spot (Vielva et al. 2004), the North-South power asymmetry, the low quadrupole moment, and the alignment of low multipoles (Huterer 2006). Additionally, f_{nl} , a measure of non-Gaussianity on the CMB, has been estimated to be positive at low significance in WMAP (Yadav & Wandelt 2008; Komatsu et al. 2008). This indicates a CMB temperature distribution that is slightly skewed toward low temperatures, as predicted by a small nonlinear ISW effect that enhances supervoid signals over superclusters (Tomita & Inoue 2007). We indeed find somewhat stronger cold spots, and although the difference is not statistically significant, its consistency

with the above picture is intriguing.

For supplementary information, including the void and cluster catalogs, see Granett et al. (2008), and <http://ifa.hawaii.edu/cosmowave/supervoids/>.

We thank Adrian Pope for useful discussions and help with the SDSS masks and catalog. We are grateful for support from NASA grant NNG06GE71G and NSF grant AMS04-0434413.

Funding for the SDSS and SDSS-II has been provided by the Alfred P. Sloan Foundation, the Participating Institutions, the National Science Foundation, the U.S. Department of Energy, the National Aeronautics and Space Administration, the Japanese Monbukagakusho, the Max Planck Society, and the Higher Education Funding Council for England. The SDSS Web Site is <http://www.sdss.org/>.

The SDSS is managed by the Astrophysical Research Consortium for the Participating Institutions. The Participating Institutions are the American Museum of Natural History, Astrophysical Institute Potsdam, University of Basel, University of Cambridge, Case Western Reserve University, University of Chicago, Drexel University, Fermilab, the Institute for Advanced Study, the Japan Participation Group, Johns Hopkins University, the Joint Institute for Nuclear Astrophysics, the Kavli Institute for Particle Astrophysics and Cosmology, the Korean Scientist Group, the Chinese Academy of Sciences (LAMOST), Los Alamos National Laboratory, the Max-Planck-Institute for Astronomy (MPIA), the Max-Planck-Institute for Astrophysics (MPA), New Mexico State University, Ohio State University, University of Pittsburgh, University of Portsmouth, Princeton University, the United States Naval Observatory, and the University of Washington.

REFERENCES

- Adelman-McCarthy, J. K., et al. 2008, *ApJS*, 175, 297
 Afshordi, N., Loh, Y.-S., & Strauss, M. A. 2004, *Phys. Rev. D*, 69, 083524
 Atrio-Barandela, F., Kashlinsky, A., Kocevski, D., & Ebeling, H. 2008, *ApJ*, 675, L57
 Blake, C., Collister, A., & Lahav, O. 2008, *MNRAS*, 385, 1257
 Boughn, S., & Crittenden, R. 2004, *Nature*, 427, 45
 Collister, A., et al. 2007, *MNRAS*, 375, 68
 Crittenden, R. G., & Turok, N. 1996, *Phys. Rev. Lett.*, 76, 575
 Eisenstein, D. J., et al. 2001, *AJ*, 122, 2267
 Giannantonio, T., Scranton, R., Crittenden, R. G., Nichol, R. C., Boughn, S. P., Myers, A. D., & Richards, G. T. 2008, *Phys. Rev. D*, 77, 123520
 Górski, K. M., Hivon, E., Banday, A. J., Wandelt, B. D., Hansen, F. K., Reinecke, M., & Bartelmann, M. 2005, *ApJ*, 622, 759
 Granett, B. R., Neyrinck, M. C., & Szapudi, I. 2008, preprint. (arXiv:0805.2974)
 Hinshaw, G., et al. 2008, *ApJS*, submitted (arXiv:0803.0732)
 Ho, S., Hirata, C. M., Padmanabhan, N., Seljak, U., & Bahcall, N. 2008, *Phys. Rev. D*, submitted (arXiv:0801.0642)
 Huterer, D. 2006, *New Astronomy Review*, 50, 868
 Inoue, K. T., & Silk, J. 2007, *ApJ*, 664, 650
 Komatsu, E., et al. 2008, *ApJS*, submitted. (arXiv:0803.0547)
 Maturi, M., Dolag, K., Waelkens, A., Springel, V., & Enßlin, T. 2007, *A&A*, 476, 83
 McEwen, J. D., Wiaux, Y., Hobson, M. P., Vanderghynst, P., & Lasenby, A. N. 2008, *MNRAS*, 384, 1289
 Neyrinck, M. C., 2008, *MNRAS*, 386, 2101
 Neyrinck, M. C., Gnedin, N. Y., & Hamilton, A. J. S. 2005, *MNRAS*, 356, 1222
 Okabe, A., Boots, B., Sugihara, K., & Chiu S.N. 2000, *Spatial Tessellations* (New York: Wiley)
 Padmanabhan, N., Hirata, C. M., Seljak, U., Schlegel, D. J., Brinkmann, J., & Schneider, D. P. 2005, *Phys. Rev. D*, 72, 043525
 Platen, E., van de Weygaert, R., & Jones, B. J. T. 2007, *MNRAS*, 380, 551
 Raccanelli, A., Bonaldi, A., Negrello, M., Matarrese, S., Tormen, G., & De Zotti, G. 2008, *MNRAS*, 386, 2161
 Rakić, A., Räsänen, S., & Schwarz, D. J. 2006, *MNRAS*, 369, L27
 Rees, M. J., & Sciama, D. W. 1968, *Nature*, 217, 511
 Rudnick, L., Brown, S., & Williams, L. R. 2007, *ApJ*, 671, 40
 Sachs, R. K., & Wolfe, A. M. 1967, *ApJ*, 147, 73
 Scranton, R., et al. 2003, preprint. (arXiv:astro-ph/0307335)
 Seljak, U. 1996, *ApJ*, 460, 549
 Springel, V., et al. 2005, *Nature*, 435, 629
 Sunyaev, R. A., & Zeldovich, Y. B. 1972, *Comments on Astrophysics and Space Physics*, 4, 173
 Tomita, K., & Inoue, K. T. 2007, preprint. (arXiv:0712.1291)
 Tuluie, R., Laguna, P., & Anninos, P. 1996, *ApJ*, 463, 15
 van de Weygaert, R., & Schaap, W. 2007, in *Data Analysis in Cosmology*, ed. V. Martínez et al. (Berlin: Springer), in press (arXiv:0708.1441)
 Vielva, P., Martínez-González, E., Barreiro, R. B., Sanz, J. L., & Cayón, L. 2004, *ApJ*, 609, 22
 Wake, D. A., et al. 2008, *MNRAS*, 387, 1045
 Yadav, A. P. S., & Wandelt, B. D. 2008, *Phys. Rev. Lett.*, 100, 181301